Nat Hazards (2018) 90:1137–1151
https://doi.org/10.1007/s11069-017-3088-8

ORIGINAL PAPER

Experimental and theoretical study on the effect of unsteady flow on the fracturing pressure in hydraulic fracturing test

Mingze Liu[1] · Guang Zhang[1] · Guogang Gou[4] · Bing Bai[2] · Shaobin Hu[3] · Xiaochun Li[2]

Received: 1 August 2017 / Accepted: 23 October 2017 / Published online: 1 November 2017
© Springer Science+Business Media B.V., part of Springer Nature 2017

Abstract Reasonable determination of formation fracturing pressure concerns the stable operation of underground fluid injection projects. In this work, we studied the effect of unsteady flow on fracturing pressure. Hydraulic fracturing tests on low permeable sandstone were conducted with the injection rate between 0.1 and 2.0 ml/min. Then, the fracturing pressure prediction models for hollow cylinder under both unsteady flow and steady flow conditions were deduced. Finally, the effect of unsteady flow on the fracturing pressure was studied based on the experimental result and several influence factors. It was shown that fracturing pressure increased with the elevated pressurization rate in the tests, while the slope of the variation curve decreases. The model considering unsteady flow can reflect the variation tendency of fracturing pressures in experiments, while fracturing pressures from the model considering steady flow are invariant with different pressurization rates. Fracturing pressure decreases with the elevated rock permeability and increases with the elevated fluid viscosity, and these two effects are actually generated by the unsteady flow. Whether to consider the unsteady flow has no significant influence on the effect of rock tensile strength on fracturing pressure when the tensile strength is very low. However, when the tensile strength is high, the effect of unsteady flow cannot be neglected.

Keywords Fracturing pressure · Hydraulic fracturing · Unsteady flow · Fluid injection

✉ Mingze Liu
mingzeliu@hotmail.com

[1] School of Resource and Environment Engineering, Wuhan University of Technology, Wuhan, China

[2] State Key Laboratory of Geomechanics and Geotechnical Engineering, Institute of Rock and Soil Mechanics, Chinese Academy of Sciences, Wuhan, China

[3] College of Civil and Transportation Engineering, Hohai University, Nanjing, China

[4] Changsha Engineering and Research Institute Ltd. of Nonferrous Metallurgy, Changsha, China

1 Introduction

Formation fracturing pressure refers to the bottom-hole pressure that is high enough to fracture the formation, including making new fractures or opening existing fractures. Reasonable determination of formation fracturing pressure concerns the stable operation of underground fluid injection projects (Bai et al. 2012; Li et al. 2015; Wei et al. 2016). The determination method of formation fracturing pressure contains direct method and indirect method. Direct method is exactly in-site hydraulic fracturing test to gain formation fracturing pressure (Ito and Hayashi 1991; Pirayesh et al. 2015). This method has the high accuracy and the high cost, so it is generally only carried out on the representative formations. Indirect methods include mathematical prediction models and prediction methods based on logging data (Anderson et al. 1973; Hongquan et al. 2004) in which the mathematical prediction models have significance for understanding the mechanism of formation fracturing and play an irreplaceable role in the prefeasibility study on projects due to its low cost.

Prediction models for formation fracturing pressure can be divided into two types, which are the models for permeable formation and the models for impermeable formation (Matthews and Kelly 1967; Pennebaker 1968; Eaton 1969; Daines 1982) in which the models for impermeable formation are not the research interest of this article, so they will not be reviewed. The original model for permeable formation was proposed by Haimson and Fairhurst (1967). It considered that the formation fracturing occurred when the tensile stress generated by crustal stress, pore pressure, wellbore fluid pressure and seepage force at the borehole wall exceeded the tensile strength of formation rock. Subsequently, some scholars developed this model. Deng et al. (2002) deduced a detailed formula for seepage force and introduced it to the prediction model. Li and Kong (2000) proposed a dual effective stress model and applied it to the prediction model. All of these models assumed that the flow of the fluid from the wellbore to the formation during the fracturing was steady in their derivation process. However, the formation fracturing is generally induced by the pressurization of wellbore fluid, and the flow with an elevated pressure source is unsteady. Many hydraulic fracturing tests on a variety of rocks were conducted (Zoback et al. 1977; Solberg et al. 1980; Wu et al. 2008). They provided experimental support for studying the effect of unsteady flow on fracturing pressure. Therefore, it is necessary to study the effect of unsteady flow on fracturing pressure based on highly accurate hydraulic fracturing test. The outcomes will contribute to the development of more advanced fracturing pressure models.

In this work, we studied the effect of unsteady flow on fracturing pressure. Hydraulic fracturing tests on low permeable sandstone were conducted with the injection rate in the range of 0.1–2.0 ml/min. Variation in fracturing pressure with pressurization rate was investigated based on the experimental results. Then, we deduced the fracturing pressure prediction models for hollow cylinder under both unsteady flow and steady flow conditions. Finally, several influence factors of the fracturing pressure were studied based on the models, and the calculated results, respectively, from the model considering unsteady flow (MUF) and the model considering steady flow (MSF) were compared and analyzed.

2 Experimental investigation

2.1 Sample introduction

The low permeable sandstone samples used in the tests, which have a good homogeneity, were bought from a quarry in Sichuan Province, China. If the sandstone has a high permeability, the hydraulic fracturing test is likely to be failed due to the rapid diffusion of internal pressure. Therefore, we chose the low permeable sandstone. They were prepared as 100-mm-long hollow cylindrical specimens with an inner diameter of 20 mm and outer diameter of 50 mm (Fig. 1). Their permeability was measured as 4.31×10^{-3} mD based on the steady flow method under confining pressure of 5 MPa and differential fluid pressure of 2 MPa between two ends of the specimen. The crystallized mineral phases of the sandstone were composed of 59.38% quartz, 9.66% kaolinite, 7.87% calcite, 7.57% dolomite, 7.41% albite, 5.23% illite and 2.88% chlorite as tested by X-ray diffraction experiment.

2.2 Experimental apparatus

All experiments were conducted in a self-developed hollow cylinder tensile tester. Figure 2 shows the schematic diagram of the tester. The device consists of a triaxial loading subsystem, a pressure chamber, a temperature control subsystem and a data acquisition subsystem.

Among them, the triaxial loading subsystem comprises of two ISCO metering pumps and a manual hydraulic pump for loading internal pressure, confining pressure or pore pressure, and axial pressure, respectively. The axial pressure is provided by the manual pump and directly imposed on the two ends of the specimen by the top and bottom disks. The confining pressure is equal to the pore pressure since the specimen is not jacketed. The ISCO metering pump can precisely control the fluid pressure and injection rate, and in real time record the data of pressure, injection rate and volume. In addition, it has two loading modes, namely constant pressure mode and constant flow rate mode. The loading of internal pressure, confining pressure and axial pressure on the hollow cylinder specimen will form a true triaxial stress state with a negative minimum principal stress, which is similar to the stress state of wellbore wall rock with the effect of maximum crustal stress, minimum crustal stress and overburden pressure.

The pressure chamber contains a top cover and a sample holder. The specimen is fixed in the center of the pressure chamber by connecting the upper and lower ends of the specimen hollow to the protuberance of the upper block and the chassis. The temperature

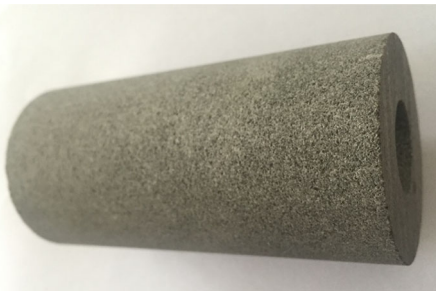

Fig. 1 Picture of the hollow cylindrical sandstone specimens

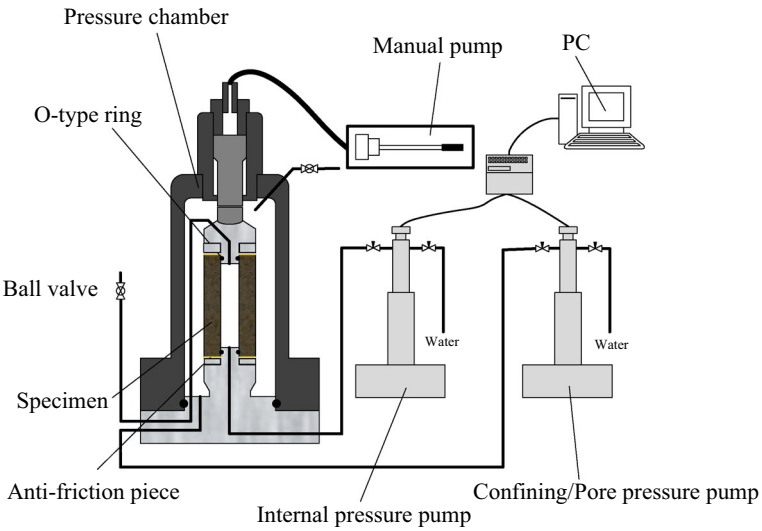

Fig. 2 Schematic diagram of hollow cylinder tensile tester

control subsystem includes a water bath sink and a circulating water bath device, in which the circulating water bath is connected to the thermostatic chamber of the pump to heat the fluids in the pump. To achieve a constant temperature, the pressure chamber is placed in the water bath sink, while the constant temperature of the fluids in metering pumps is realized by the circulating water bath device. The data acquisition subsystem included a pressure gauge of the manual oil hydraulic pump, a water bath thermometer, a pressure sensor, a flow sensor, a volume sensor on the metering pump and a recording software. The pressure sensor, the flow sensor and the volume sensor were installed on the top of the ISCO metering pump, which can collect the data of the metering pump's pressure, flow and volume at a sampling frequency of 2.0 Hz. The acquired data were subsequently transmitted to the computer and recorded in real time by the ISCO control software. The overall pressure endurance ability of this apparatus is 50 MPa. In addition, copper sheet and PTFE film were used as the anti-friction pieces to decrease the end friction effect of the specimen.

2.3 Experimental scheme

Hydraulic fracturing tests under different injection rate condition were designed since the formation fracturing occurs in the fluid pressurization process caused by fluid injection. The injection rates were set as 0.1, 0.2, 0.3, 0.5, 0.8, 1.0, 1.5, 2.0 ml/min, respectively. The injection rates were determined based on the property of the apparatus and experimental experience. All the tests were carried out at an axial pressure of 20 MPa. The axial pressure is used to seal the fluid of internal pressure and has no influence on the experimental result. The initial internal pressure, which is the pressure that internal pressure begins to increase during the injection, confining pressure and pore pressure were all set as 3.0 MPa. The pressurization rate in each test can be calculated using fracturing pressure to divide injection time based on the pressure curve. The experiments were performed under room temperature.

2.4 Experimental procedures

The experimental procedure included three steps: (1) specimen installation; (2) pressure preloading; and (3) specimen fracturing. For sample installation, the specimen was installed into the rock core holder. Then, the pipelines were connected and the top cover of the pressure chamber was fixed. For pressure preloading, triaxial loading subsystem was connected to the pressure chamber after the installation of the specimen. The axial pressure was loaded on the specimen by the manual hydraulic pump. The confining pressure chamber was then filled with distilled water by ISCO pump to load confining pressure. After loading confining pressure, the internal pressure and the pore pressure would be gradually equal to the confining pressure due to the connection between the internal pressure chamber and the confining pressure chamber through the pore system of the specimen. For specimen fracturing, fluid was injected into the internal pressure chamber by ISCO pump at a certain rate to increase internal pressure. In this process, the confining pressure pump was controlled in constant pressure mode. The injected fluid would flow from the internal pressure chamber to the confining pressure chamber through the specimen. When the pressure reading of the internal pressure pump suddenly dropped, the specimen was considered being fractured.

3 Experimental results

3.1 Fracturing process

Figure 3 shows the variation in internal pressure and confining pressure with time in the hydraulic fracturing test with 0.2 ml/min injection rate. We take this test for example to describe the fracturing process. The orange curve in the figure represents the variation in internal pressure. It is indicated that the internal pressure increased from 3.0 MPa with time. As the rock permeability is low, the injected fluid could not rapidly diffuse, inducing

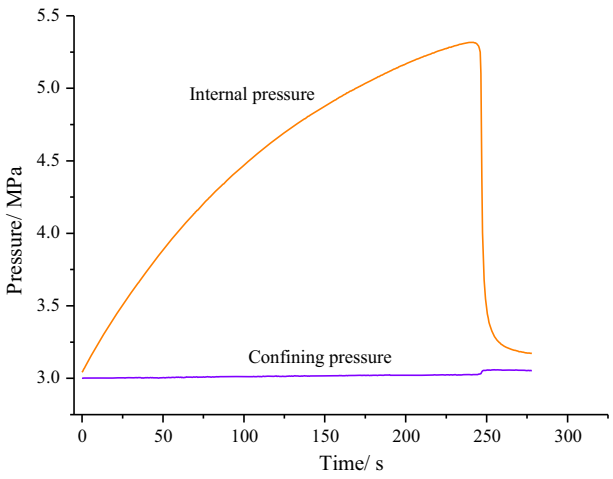

Fig. 3 Variation in internal pressure and confining pressure with time in the hydraulic fracturing test with 0.2 ml/min injection rate

the increase in the internal pressure. The internal pressure increased from 3.0 to 5.32 MPa at 242 s and then suddenly dropped to 3.18 MPa. This is because that the tensile failure occurred, a crack connecting the inner surface and outer surface of the specimen was generated, resulting in the dissipating of internal pressure. Therefore, we regarded the peak pressure point of the curve as the fracturing pressure. The purple curve represents the variation in confining pressure. The confining pressure pump was in constant pressure mode during the test. So when the confining pressure is not the set value, the pump will automatically control the piston to move forward or backward to adjust the pressure to the set value. However, there is a delay in the adjustment of pressure, so the confining pressure shows a slight upward trend before fracturing. Then, the confining pressure suddenly increased to 3.05 MPa. This is because much fluid flowed to the confining pressure chamber due to the fracturing of the specimen at 242 s. As the volume of the confining pressure chamber is much greater than the volume of the internal pressure chamber, the variation in the confining pressure is much smaller than the internal pressure. It is also demonstrated in the figure that the internal pressure was still 0.13 MPa higher than the confining pressure after the fracturing. This is because the resistance of the fluid flowing along the crack generated a certain pressure drop.

Figure 4 shows the flow rate of the internal pressure pump and the confining pressure pump varying with time in the hydraulic fracturing test with 0.2 ml/min injection rate. The orange curve in the figure represents the variation in the flow rate of internal pressure pump. It is indicated that the flow rate of internal pressure pump kept constant at 0.2 ml/min due to the constant flow rate mode. The purple curve represents the variation in the flow rate of confining pressure pump. As the pump was in the constant pressure mode, when the fluid in the internal pressure chamber flowed to the confining pressure chamber through the specimen, the piston of the pump was controlled to move backward to adjust the pressure and generated the negative flow rate. The greater the difference between the actual pressure and the set value was, the larger the flow rate to adjust the pressure was. Therefore, the flow rate of the confining pressure pump reflects the seepage velocity of the fluid through the specimen. It is showed that the absolute value of the flow rate of the confining pressure pump increases with time. This is due to that the difference in the

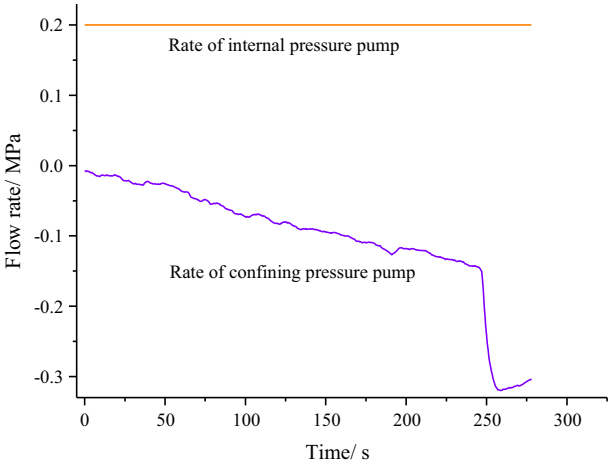

Fig. 4 Flow rate of the internal pressure pump and the confining pressure pump varying with time in the hydraulic fracturing test with 0.2 ml/min injection rate

internal pressure and confining pressure increased with time, inducing the increase in the seepage velocity according to the Darcy law. The flow rate of confining pressure pump decreased from 0 to − 0.14 ml/min before fracturing. When fracturing occurred at time 242 s, much fluid flowed to confining pressure chamber, causing the rapid decrease in the pump flow rate. The maximum negative flow rate was − 0.32 ml/min at time 258 s.

3.2 Hydraulic fracturing results

Figure 5 shows the variation in internal pressure with time in the hydraulic fracturing tests under eight sets of injection rate conditions. The shape of each curve in the figure is similar. However, their pressurization rates are quite different, especially at 0.1 ml/min injection rate condition, which is much lower than the others. The peak value of each pressure curve was regarded as the fracturing pressure. The pressurization rates were calculated by dividing the fracturing pressure by time. Figure 6 shows the variation in fracturing pressure with pressurization rate. It is revealed that the fracturing pressure increases with pressurization rate on the whole. But the slope of the variation decreases with the pressurization rate. The minimum fracturing pressure was 5.01 MPa at the pressurization rate of 0.0075 MPa/s, while the maximum fracturing pressure was 6.00 MPa at the pressurization rate of 0.131 MPa/s. The experimental conditions and results of the tests are shown in Table 1.

4 Theoretical analysis

4.1 Prediction models of fracturing pressure for hollow cylinder

According to current studies on fracturing pressure prediction models, they considered that the formation fracturing occurred when the tensile stress generated by crustal stress, pore pressure, wellbore fluid pressure and seepage force at the borehole wall exceeded the tensile strength of formation rock. Hydraulic fracturing of hollow cylinder specimen in this

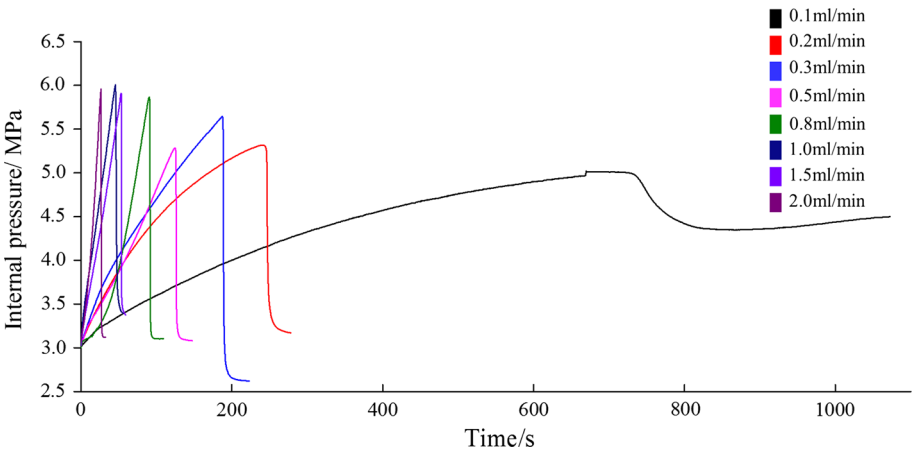

Fig. 5 Variation in internal pressure with time in the hydraulic fracturing tests under eight sets of injection rate condition

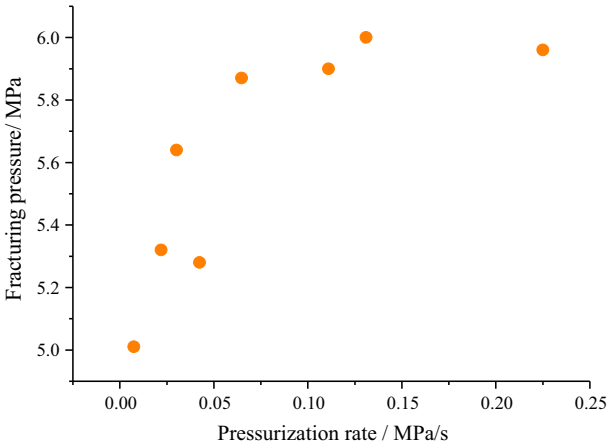

Fig. 6 Variation in fracturing pressure with pressurization rate

Table 1 Experimental conditions and results

No.	Injection rate (ml/min)	Pressurization rate (MPa/s)	Fracturing pressure (MPa)
1	0.1	0.00750	5.01
2	0.2	0.0220	5.32
3	0.3	0.0302	5.64
4	0.5	0.0424	5.28
5	0.8	0.0648	5.87
6	1.0	0.131	6.00
7	1.5	0.111	5.90
8	2.0	0.225	5.96

work is quite similar to the formation fracturing, excepting that the crustal stress is replaced by confining pressure. Besides, there are many natural cracks in rock. The tensile fracturing of rock is actually the propagation of micro-cracks. This is also the basic assumption of fracture mechanics (Shah et al. 1995). We believe that this assumption is more reasonable than the assumption that the fracturing initiates at the rock surface, which was adopted in the conventional formation fracturing pressure prediction models. Therefore, for the hollow cylinder specimen in this work, we assumed that when the tensile stress generated by the confining pressure, pore pressure, internal pressure and seepage force at the tip of the natural crack exceeded the rock tensile strength, the specimen fracturing occurred.

The tensile stress at the tip of the crack for hollow cylinder consists of three parts: (1) tensile stress generated by internal pressure and confining pressure; (2) pore fluid pressure; and (3) tensile stress generated by seepage force. They are expressed as:

$$\sigma_c = \sigma_c^f + \sigma_c^p + \sigma_c^s \tag{1}$$

where σ_c^f is the tensile stress generated by internal pressure and confining pressure, MPa; σ_c^p is the pore fluid pressure, MPa; σ_c^s is the tensile stress generated by seepage force, MPa. These parts were analyzed below in detail.

Tensile stress generated by internal pressure and confining pressure was calculated by Lame's formula, which was deduced based on elastic mechanics to calculate the circumferential stress and the radial stress of any point in hollow cylinder. It is expressed as:

$$\begin{cases} \sigma_r = \dfrac{P_2R_2^2 - P_1R_1^2}{R_2^2 - R_1^2} - \dfrac{(P_2 - P_1)R_1^2R_2^2}{r^2\left(R_2^2 - R_1^2\right)} \\ \sigma_\theta = \dfrac{P_2R_2^2 - P_1R_1^2}{R_2^2 - R_1^2} + \dfrac{(P_2 - P_1)R_1^2R_2^2}{r^2\left(R_2^2 - R_1^2\right)} \end{cases} \tag{2}$$

where σ_r is the radial stress, MPa; P_2 is the confining pressure, MPa; R_2 is the external radius, m; P_1 is the internal pressure, MPa; R_1 is the internal radius, m; r is the radius of calculated point; σ_θ is the circumferential stress, MPa.

We introduced a parameter named natural crack length, which is expressed by λ. The formula for calculating the circumferential tensile stress at the crack tip was subsequently obtained based on Eq. (2) as follows:

$$\sigma_c^f = \frac{P_2R_2^2 - P_1R_1^2}{R_2^2 - R_1^2} + \frac{(P_2 - P_1)R_1^2R_2^2}{(R_1 + \lambda)^2\left(R_2^2 - R_1^2\right)} \tag{3}$$

To get the pore pressure at the crack tip, we have to deduce the distribution function of pore pressure for hollow cylinder.

First, we assumed the fluid flow through the specimen to be unsteady. The distribution function of pore pressure for plane radial flow problem is too complex for subsequently solving the equations for fracturing pressure. Hence, we simplified the problem to be a one-dimensional flow problem. There is a differential equation for this problem (Carslaw and Jaeger 1959) as follows:

$$\frac{\partial^2 P}{\partial x^2} = \frac{1}{c}\frac{\partial P}{\partial t} \tag{4}$$

where P is the pressure, MPa; x is the distance, m; c is the pressure conductivity coefficient of formation, m^2/s, which is calculated as:

$$c = \frac{k}{c_t\mu} \tag{5}$$

where k is the permeability, m^2; c_t is the total compressibility, MPa^{-1}; μ is the fluid viscosity, Pa s.

Equation (4) satisfies the following boundary conditions:

$$\begin{cases} x = 0, & P = P_1 \\ t = 0, & P = P_2 \end{cases} \tag{6}$$

Solution of Eq. (4) is:

$$P = (P_1 - P_2)\,\mathrm{erfc}\left(\frac{x}{2\sqrt{ct}}\right) + P_2 \tag{7}$$

The internal pressure was assumed to increasing with time at a constant rate, so there is: $P_1 = P_2 + At$. Therefore, we obtained the distribution function of pore pressure at the crack tip considering unsteady flow:

$$P_{\text{uns}}(\lambda, t) = At\,\text{erfc}\left(\frac{\lambda}{2\sqrt{ct}}\right) + P_2 \tag{8}$$

Then, we assumed the fluid flow through the specimen to be stable to compare with the unsteady condition. The flow was also simplified as a one-dimensional flow problem for convenient comparison. There is also a differential equation for this problem as follows:

$$\frac{\mathrm{d}^2 P}{\mathrm{d}x^2} = 0 \tag{9}$$

Equation (9) satisfies the following boundary conditions:

$$\begin{cases} x = 0, & P = P_1 \\ x = R_2 - R_1, & P = P_2 \end{cases} \tag{10}$$

Solutions of Eq. (9) is:

$$P = \frac{P_2 - P_1}{R_2 - R_1} x + P_1 \tag{11}$$

The distribution function of pore pressure at the crack tip considering steady flow was:

$$P_s(\lambda, t) = \left(1 - \frac{\lambda}{R_2 - R_1}\right) At + P_2 \tag{12}$$

Thus, we, respectively, deduced the distribution function of pore pressure at the crack tip under unsteady and steady flow conditions with a constant internal pressure. However, the actual internal pressure increased with time. So the distribution function of pore pressure with an elevated internal pressure was deduced using the weight function as follows:

$$\sigma_c^p = P_a(\lambda, t) = \frac{1}{t_0} \int_0^{t_0} P(\lambda, t)\,\mathrm{d}t \tag{13}$$

where t_0 is the time of pressurization (s) and $P(\lambda, t)$ is the distribution function of pore pressure with a constant internal pressure. It is Eq. (8) under unsteady flow condition and changes to formula (12) under steady flow condition.

For the calculation of the seepage force, Detournay and Cheng (1993) proposed a simple calculation formula as follows:

$$\sigma_s = -2\eta(P - P_2) \tag{14}$$

where P is the pore pressure, MPa, and η is in the range of 0–0.5 and is calculated by the following equation:

$$\eta = \frac{\alpha(1 - 2v)}{2(1 - v)} \tag{15}$$

where α is the Biot coefficient and v is the Poisson's ratio.

Thus, the equation for seepage force is as follows:

$$\sigma_c^s = -\frac{\alpha(1-2v)}{(1-v)}(P_a(\lambda, t) - P_2) \tag{16}$$

According to the assumption, the fracturing occurs when the tensile stress at the crack tip exceeds the rock tensile strength. Therefore, the criterion of fracturing is as follows:

$$\sigma_c^f + \sigma_c^p + \sigma_c^s = T \tag{17}$$

Based on Eq. (17), the time node t_0 of the fracturing was acquired. The fracturing pressure was finally obtained by substituting t_0 to $P_1 = P_2 + At$.

Therefore, the MUF and MSF were introduced by the above derivation. Their main difference was the calculation of the distribution function for pore pressure. For unsteady flow, it was calculated by Eq. (8), while the pore pressure of steady flow was calculated by Eq. (12).

4.2 Comparison of theoretical results and experimental results

In this section, to verify the models deduced in Sect. 4.1, we compared the calculated results from MUF and MSF with the experimental results. The parameter values used in the calculation are listed in Table 2 in which the pore pressure value was from the experimental condition; the pressurization rate value was calculated based on the pressure curve; the natural crack length value was estimated; the Biot coefficient, Poisson's ratio and rock tensile stress values were estimated based on the mechanics parameters of the analogous rocks (Jaeger et al. 2009); the permeability value was estimated from the laboratory test; the viscosity value of the water was estimated from NIST Web site.

Figure 7 shows the variation in fracturing pressures, which were, respectively, from experiments, MUF and MSF, with time. It is demonstrated that the MUF is capable of reflecting the variation tendency of fracturing pressure in the experiments, while fracturing pressures from the MSF are invariant with different pressurization rates and were equal to the value from MUF at the pressurization rate of 0.04 MPa/s. Therefore, it is suggested that the MUF has more advantages than MSF.

Table 2 Parameter values list for the models

Parameter	Value
Pore pressure P_2/MPa	3.0
Pressurization rate A/MPa/s	Based on tests
Natural crack length λ/m	0.008
Biot coefficient α	0.1
Poisson's ratio v	0.45
Internal radius R_1/m	0.01
External radius R_2/m	0.025
Permeability k/m^2	4.31×10^{-18}
Viscosity μ/Pa s	8.8899×10^{-4}
Tensile stress T/MPa	1.85

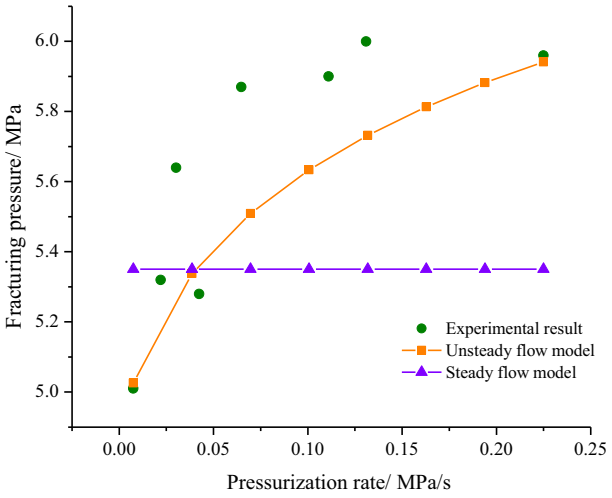

Fig. 7 Variation in fracturing pressures, which were, respectively, from experiments, prediction model considering unsteady flow, prediction model considering steady flow, with time

5 Study of influence factors

In this section, we studied the effect of rock permeability, rock tensile strength and fluid viscosity on the fracturing pressure based on the MUF. Furthermore, results from the MSF were compared with MUF to study the effect of unsteady flow on these factors. The pressurization rate in the below studies was set as 0.1 MPa/s, and other parameters were the same as shown in Table 2.

5.1 Effect of rock permeability

Rock permeability is a significant property of formation and substantially varies with injection sites and rock types. Figure 8 shows the variation in fracturing pressure with rock permeability in the range of 1×10^{-18}–5×10^{-18} m^2. It is indicated that the fracturing

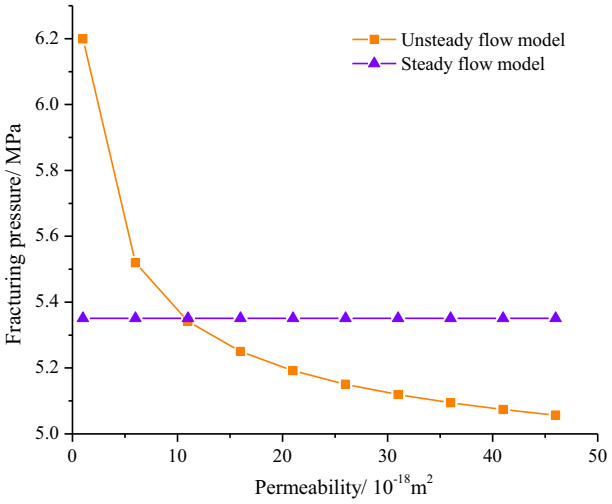

Fig. 8 Variation in fracturing pressure with the rock permeability in the range of 1×10^{-18}–5×10^{-18} m^2

pressure decreases with the increase in the rock permeability and then gradually approaches a steady. But the results from the MSF are invariant with the rock permeability. Therefore, it is suggested that the effect of rock permeability on fracturing pressure is actually generated by the unsteady flow.

5.2 Effect of rock tensile strength

Tensile strength is the major property of rock that controls the tensile fracturing, and it is influenced by the stress state of rock including confining pressure (Al-Shayea et al. 2000; Funatsu et al. 2014), which is actually the crustal stress for formation rock. Hence, the tensile strength used in formation prediction models is different from that measured in conventional tests such as direct tensile test and Brazilian split test. As a result, it is difficult to be determined and necessary to be studied. Figure 9 shows the variation in fracturing pressure with rock tensile strength in the range of 0.1–9.1 MPa. It is indicated that the fracturing pressure increases approximately linearly with the elevated rock tensile strength. Besides, the difference in MSF and MUF is negligible with tensile strength lower than 4.84 MPa, but gradually increases with tensile strength greater than 4.84 MPa. Therefore, whether to consider the unsteady flow has no significant influence on the effect of rock tensile strength on fracturing pressure when the tensile strength is very low. However, when the tensile strength is high, the effect of unsteady flow cannot be neglected.

5.3 Effect of fluid viscosity

Many underground fluid injection projects inject various fluids, including water, CO_2, CH_4, N_2 (Panfilov et al. 2006; Orr 2009; Wei and Li 2011). The viscosity of these fluids varies not only with fluid type, but also with the phase state. Therefore, it is necessary to study the effect of fluid viscosity on fracturing pressure. Figure 10 shows the variation in fracturing pressure with fluid viscosity in the range of 1.0×10^{-6}–9.1×10^{-5} Pa s. It is revealed that the fracturing pressure increases with the increase in the fluid viscosity. But the results from the MSF are invariant with the fluid viscosity. Besides, the results of MSF were all

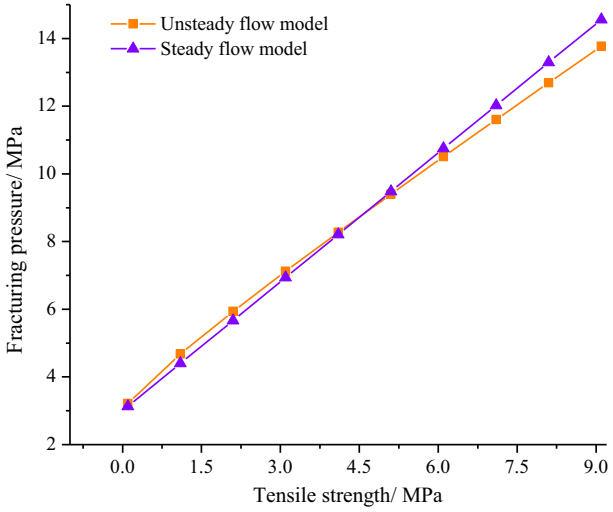

Fig. 9 Variation in fracturing pressure with rock tensile stress in the range of 0.1–9.1 MPa

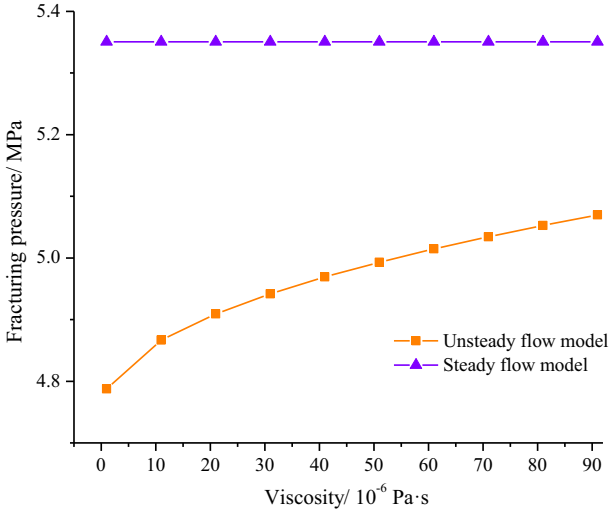

Fig. 10 Variation in fracturing pressure with fluid viscosity in the range of 1.0×10^{-6}–9.1×10^{-5} Pa s

obviously higher than the results of MUF. Hence, consideration of unsteady flow contributes to reflect the effect of fluid viscosity on the fracturing pressure.

6 Conclusions

In this work, hydraulic fracturing tests on low permeable sandstone were conducted with the injection rate in the range of 0.1–2.0 ml/min. Variation in fracturing pressure with pressurization rate was investigated based on the experiments. The fracturing pressure prediction models for hollow cylinder under both unsteady flow and steady flow conditions were, respectively, deduced. The effect of unsteady flow on the fracturing pressure was studied based on the experimental result and several influence factors. The main conclusions are as follows:

1. Fracturing pressure increased with the elevated pressurization rate in the tests, while the slope of the variation curve decreases. The MUF is capable of reflecting the variation tendency of fracturing pressures in experiments, while fracturing pressures from the MSF are invariant with different pressurization rates. This is because the MUF considered the pore pressure distribution under unsteady flow condition. Therefore, it is suggested that the MUF has more advantages than MSF.
2. Based on the calculation results of MUF, fracturing pressure decreases with the elevated rock permeability and increases with the elevated fluid viscosity, while the fracturing pressures calculated from the MSF model were invariant with both rock permeability and fluid viscosity. Therefore, it is suggested that the consideration of unsteady flow reflects the effect of rock permeability and fluid viscosity on fracturing pressure.
3. Fracturing pressure increases linearly with the rock tensile strength. When the tensile strength is very low, whether to consider the unsteady flow has no significant influence on the effect of rock tensile strength on fracturing pressure. However, when the tensile strength is high, the effect of unsteady flow cannot be neglected.

Acknowledgements This work was supported by China Postdoctoral Science Foundation (Grant Numbers 2016M602381).

References

Al-Shayea NA, Khan K, Abduljauwad SN (2000) Effects of confining pressure and temperature on mixed-mode (I–II) fracture toughness of a limestone rock. Int J Rock Mech Min Sci 37:629–643. https://doi.org/10.1016/S1365-1609(00)00003-4

Anderson RA, Ingram DS, Zanier AM (1973) Determining fracture pressure gradients from well logs. J Pet Technol 25:1–259

Bai B, Li X, Liu M et al (2012) A fast explicit finite difference method for determination of wellhead injection pressure. J Cent South Univ 19:3266–3272

Carslaw HS, Jaeger JC (1959) Conduction of heat in solids. Clarendon Press, Oxford

Daines SR (1982) Prediction of fracture pressures for wildcat wells. J Pet Technol 34:863–872

Deng J, Wang J, Zhou J (2002) Calculation model of borehole collapse and fracture pressure in permeable formation. Chin J Rock Mech Eng 21:2069–2072

Detournay E, Cheng H-D (1993) Fundamentals of poroelasticity. In: Hudson JA (ed) Comprehensive rock engineering, vol 1. Oxford, Pergamon, pp 395–412

Eaton BA (1969) Fracture gradient prediction and its application in oilfield operations. J Pet Technol 21:1–353

Funatsu T, Kuruppu M, Matsui K (2014) Effects of temperature and confining pressure on mixed-mode (I–II) and mode II fracture toughness of Kimachi sandstone. Int J Rock Mech Min Sci 67:1–8

Haimson B, Fairhurst C (1967) Initiation and extension of hydraulic fractures in rocks. Soc Pet Eng J 7:310–318

Hongquan X, Yuanze Z, Ping C et al (2004) Log prediction of carbonate formation breakdown pressure. Nat Gas Ind 24:32–35

Ito T, Hayashi K (1991) Physical background to the breakdown pressure in hydraulic fracturing tectonic stress measurements. Int J Rock Mech Min Sci Geomech Abstr 28:285–293

Jaeger JC, Cook NG, Zimmerman R (2009) Fundamentals of rock mechanics. Wiley, New York

Li C, Kong X (2000) A theoretical study on rock breakdown pressure calculation equations of fracturing process. Oil Drill Prod Technol 22:54–56

Li Q, Lin B, Zhai C (2015) A new technique for preventing and controlling coal and gas outburst hazard with pulse hydraulic fracturing: a case study in Yuwu coal mine, China. Nat Hazards 75:2931–2946. https://doi.org/10.1007/s11069-014-1469-9

Matthews WR, Kelly J (1967) How to predict formation pressure and fracture gradient. Oil Gas J 65:92–106

Orr FM (2009) Onshore geologic storage of CO2. Science 325:1656–1658

Panfilov M, Gravier G, Fillacier S (2006) Underground storage of H2 and H2-CO2-CH4 mixtures. In: ECMOR X-10th European conference on the mathematics of oil recovery

Pennebaker ES (1968) An engineering interpretation of seismic data. Soc Pet Eng. https://doi.org/10.2118/2165-MS

Pirayesh E, Soliman MY, Rafiee M, Jamali A (2015) A new method to interpret fracturing pressure-application to frac pack. SPE J 20:508–517

Shah SP, Swartz SE, Ouyang C (1995) Fracture mechanics of concrete: applications of fracture mechanics to concrete, rock and other quasi-brittle materials. Wiley, New York

Solberg P, Lockner D, Byerlee JD (1980) Hydraulic fracturing in granite under geothermal conditions. Int J Rock Mech Min Sci Geomech Abstr. 17:25–33

Wei N, Li XC (2011) Numerical studies on the aquifer storage of CO2 containing N2. Energy Procedia 4:4314–4322

Wei X, Li Q, Li X, Sun Y (2016) Impact indicators for caprock integrity and induced seismicity in CO2 geosequestration: insights from uncertainty analyses. Nat Hazards 81:1–21. https://doi.org/10.1007/s11069-015-2063-5

Wu H, Golovin E, Shulkin Y, et al (2008) Observations of hydraulic fracture initiation and propagation in a brittle polymer. In: The 42nd US rock mechanics symposium (USRMS). American Rock Mechanics Association, Washington

Zoback MD, Rummel F, Jung R, Raleigh CB (1977) Laboratory hydraulic fracturing experiments in intact and pre-fractured rock. Int J Rock Mech Min Sci Geomech Abstr. 14:49–58